Radial anisotropy from a geometric viewpoint: Topological singularity and effective medium realization

Yong-Liang Zhang,[1] John B. Pendry,[2] and Dang Yuan Lei[1,3,*]

[1]*Department of Applied Physics, The Hong Kong Polytechnic University, Hong Kong, China*

[2]*The Blackett Laboratory, Department of Physics, Imperial College London, London SW7 2AZ, United Kingdom*

[3]*Shenzhen Research Institute, The Hong Kong Polytechnic University, Shenzhen, China*

(Received 21 February 2017; published 21 July 2017)

The correspondence between curved space-times and inhomogeneous dielectrics has been recently explored as a powerful tool to understand and manipulate novel electromagnetic behaviors in complex media. Here, we present a theoretical investigation on the optics of radially anisotropic material from a geometric viewpoint. Within the framework of transformation optics, we show that the optical medium with radial anisotropy is equivalent to a disclination geometry, which is a line topological defect carrying singular curvature. By introducing a geometric parameter characterizing the global topology of the disclination space, we systematically analyze the effective geometry and the topological charge associated with two typical radial anisotropies consisting of concentric multilayers or symmetric slices in both elliptical and hyperbolical regions. It is shown that elliptical and hyperbolic radial anisotropies give rise to optical Riemannian and pseudo-Riemannian geometries, respectively. Moreover, we investigate the wave optics as well as the semiclassical ray dynamics of light in the metamaterials at optical wavelengths from the perspective of coordinate transformation. It is found that the singularity acts on the light with an attractive or repulsive inverse cube force, depending on the topological charge. Our theory provides a simple and unified framework for light in optical media of various radial anisotropies and may shed new light on the dynamics of classical and quantum waves in topological nontrivial space.

DOI: 10.1103/PhysRevB.96.035430

I. INTRODUCTION

Radial anisotropy refers to the optical medium whose constituent tensors $\boldsymbol{\varepsilon}$ and/or $\boldsymbol{\mu}$ are diagonal in cylindrical or spherical coordinates. Since its inception in the early 1970s, radial anisotropy has been initially bound to the study of the far-field response of spherical particles coated with oriented molecule layers in bioengineering [1], anisotropic hollow particles [2], and microdroplets of nematic liquid crystal [3,4]. Over the past few years, however, there has been a renewed interest in analyzing and understanding the anomalous response of electromagnetic waves in radially anisotropic media in the research field of metamaterials. Benefiting from the conceptual development of the effective medium theory as well as the technical advances in micro- and nanofabrication, radially anisotropic metamaterials ranging from microwave to visible region have been experimentally implemented in cylindrically or spherically subwavelength concentrically multilayered or radially symmetric sliced structures. The electromagnetic response of radially anisotropic material has attracted intensive research interest for both fundamental and application reasons. One of the most intriguing features of the radial anisotropy stems from the fact that the dispersion relation of the radially anisotropic material can be engineered to some unprecedented, extreme forms by artificially tailoring the principal values of the constituent tensors. In particular, the isofrequency surface of transverse magnetic (TM) polarized waves becomes hyperbolic if the principal components of the permittivity or permeability tensor are of opposite signs [5,6]. The hyperbolically radial anisotropy enables the conversion from evanescent waves to propagating waves, thereby breaking the diffraction limit of classical optics for far-field superresolution imaging [7–10]. Moreover, homogeneous and inhomogeneous radial anisotropies have also found applications in various areas such as electromagnetic cloaking [11–13], extraordinary scattering [14–16], and anomalous absorption [17].

In the present work, within the framework of transformation optics [18–20], we present a geometric theory for the electromagnetic response of cylindrically radial anisotropy with both elliptical and hyperbolic responses. Transformation optics, which roots on the formal invariance of Maxwell's equations under holonomic spatial coordinate transformation, provides a powerful approach for novel electromagnetic device design and deep understanding of the behaviors of electromagnetic waves in homogeneous and inhomogeneous media or subwavelength plasmonic nanostructures [21] with the wave phenomena in curved space. Although there have been a great deal of theoretical and experimental investigations, including physical applications [20–28] together with theoretical extensions [29–36], most previous reports have utilized continuous, integrable coordinate transformations, which preserve the space topology upon the transformations. Perhaps an exception is the work of Horsley [37], where a two-dimensional (2D) index singularity was mimicked by a sculpted surface of low contrast, isotropic material. So, it is interesting to investigate the physical effects of novel coordinate transformations with topological singularities in physical space. In this work, we theoretically demonstrate that the optical medium, with either ordinary elliptically or hyperbolically radial anisotropy, represents a class of topologically nontrivial curved spaces, which are known as disclinations in condensed matter physics and cosmic strings cosmology [38–40]. Disclinations are one-dimensional topological defects carrying curvature singularity in the origin. Previously, we have analyzed the topological nature of the transformed

*Corresponding author: dylei@polyu.edu.hk

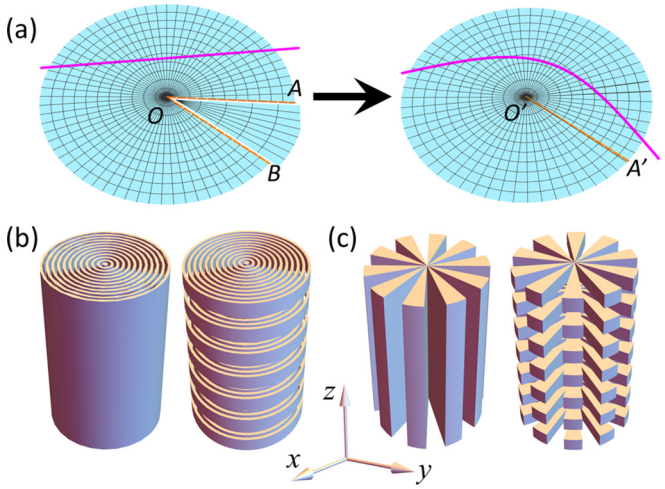

FIG. 1. (a) Schematic construction of a disclination space with the angular coordinate transformation of a Volterra process: removing a sector AOB from a flat space and gluing the remaining part by sticking the boundaries OA and OB. (b, c) The metamaterial realization of cylindrically radial anisotropies based on concentric multilayers (b) and symmetric slices (c), which are continuous or periodic, respectively.

space and the propagation of light inside the transformation medium of disclination in the elliptical region [41]. In this work, we further demonstrate that metamaterials with cylindrically radial anisotropy are geometrically equivalent with the curved spaces of disclinations, and we investigate the effective geometry for various metamaterial realizations of both elliptical and hyperbolic responses. Our motivation comes from the relationship between the radially anisotropic metamaterials and their stratified counterparts with uniaxial Cartesian anisotropy. In general, there are two types of Cartesian anisotropies with principal values $\varepsilon_{\parallel}$ and $\varepsilon_{\perp}$ [5,6], which consist of either periodically stacked flat multilayers or arrays of parallel nanowires. Geometrically, the radially anisotropic counterparts based on the effective medium of periodically concentric multilayers or symmetric slices with ε_r and ε_θ can be created by a combined cut and glue process from the uniaxial Cartesian anisotropy. For instance, removing a sector with a deficit angle $\Delta\theta = 2\pi\alpha$, $(0 < \alpha < 1)$ from a stratified parallel multilayered medium, as shown in Fig. 1(a), and gluing the remaining part by sticking the two dashed boundaries together leads to the radially anisotropic structure of concentrically multilayered shells shown in Fig. 1(b). Similarly, Fig. 1(c) illustrates the construction of another type of radial anisotropy consisting of radially symmetric slices from a parallel nanowire array structure. Note that the proposed angular transformation does not depend on the z coordinate. Consequently, ε_z can take any constant value, and the metamaterial can be either homogeneous or periodic [23,42] along the z direction, as can be seen in the right panels of Figs. 1(b) and 1(c). The above construction is reminiscent of the classical Volterra's cut and glue process in elastic or crystalline solids where applying the cut and glue process to a continuum leads to a line topological defect such as dislocation or disclination, which breaks the translational or rotational spatial symmetry [38,39]. As a result, a straight light ray in the flat space is bent under the coordinate transformation [see the purple lines in Fig. 1(a)]. As previously pointed out in [41], the Volterra construction of disclination defines a linear coordinate transformation in angular coordinates from a trivial flat space to a topological nontrivial curved space by removing or inserting a sector from the initial space, resulting in an effective conelike space for the electromagnetic waves. Here, we show that the ratio between the principal anisotropic parameters ε_r and ε_θ defines a geometric parameter α, which determines the spatial geometry and controls the dynamics of the light rays and the electromagnetic waves in the radially anisotropic medium. Moreover, the value of α for the metamaterial can be either real or imaginary, depending on the geometry and the working frequency for dispersive materials. The geometric interpretation of the radial anisotropy provides a unified description of light propagation in an ordinary or hyperbolically radial anisotropic medium, revealing the deep connection between transformation optics and a topologically nontrivial optical medium. The proposed scheme will not only provide a geometric interpretation of the optics of elliptically and hyperbolically radial anisotropies, but it will also allow applications beyond conventional transformation optics.

II. GEOMETRY OF THE RADIAL ANISOTROPY

The radial anisotropy is characterized by a diagonal permittivity or permeability tensor in cylindrical or spherical coordinates. Here, we only focus on the cylindrically anisotropic permittivity with principal values ε_r and ε_θ for simplicity and because it can be readily realized with subwavelength dielectric or metallic inclusions [6,7]. The other component of the permittivity, ε_z, can take any constant value. Without loss of generality, we introduce a geometric parameter α from the ratio between the principal parts:

$$\alpha^2 = \frac{\varepsilon_r}{\varepsilon_\theta}. \tag{1}$$

Here, we neglect the imaginary part of the permittivity in all the geometric analyses, since the metric tensors in Riemannian and pseudo-Riemannian geometry are assumed to be real. It is evident that α^2 is positive for a medium with an ordinary elliptically dielectric response (ε_r and $\varepsilon_\theta > 0$), while it is negative when the medium has a hyperbolic response where either ε_r or ε_θ is negative. Note that α is imaginary for the hyperbolic case, which corresponds to the constituent medium for the hyperlens.

For simplicity, we assume that all the ε_r, ε_θ, and α values are independent from the cylindrical coordinates (r,θ,z). Under this assumption, the radially anisotropic medium can be described in curved geometry with the following line element:

$$ds^2 = dr^2 + \alpha^2 r^2 d\theta^2 + \beta^2 dz^2, \tag{2}$$

where β is a real constant, the only nonzero components of the metric tensor are $g_{rr} = 1$, $g_{zz} = \beta^2$, and $g_{\theta\theta} = \alpha^2 r^2$, and the other components vanish identically. For $\alpha > 0$, above metric has a simple intuitive interpretation of the disclination in solids or the spatial part of space outside of the cosmic strings. To understand the geometry of the radial anisotropy, we compare the interval in Eq. (2) with the line element in flat space: $ds^2 = dr^2 + r^2 d\theta^2 + dz^2$. It is easily to find that the interval

in Eq. (2) can be obtained by the following transformation on the angular coordinate:

$$r' = r, \quad \theta' = \alpha\theta, \quad z' = \beta z. \tag{3}$$

Keeping the product $\boldsymbol{\varepsilon} \times \mu^{zz}$ invariant to satisfy the nonmagnetic condition, the transformed permittivity in Cartesian coordinates corresponding to Eq. (3) takes the following form,

$$\boldsymbol{\varepsilon} = \begin{pmatrix} \sin^2\theta + \alpha^2\cos^2\theta & \sin\theta\cos\theta(\alpha^2-1) & 0 \\ \sin\theta\cos\theta(\alpha^2-1) & \sin^2\theta + \alpha^2\cos^2\theta & 0 \\ 0 & 0 & \alpha^2/\beta^2 \end{pmatrix} \varepsilon_i. \tag{4}$$

If we only consider that the incident wave is TM polarized, the permittivity in Eq. (4) can be diagonalized in cylindrical coordinates to

$$\varepsilon_\theta = \varepsilon_i, \quad \varepsilon_r = \alpha^2\varepsilon_i. \tag{5}$$

At the same time, the z component ε_z can take any constant value by assuming a nontrivial background material or simply tailoring β. Therefore, the radial anisotropy can be interpreted as the curved geometry of the disclination with coordinate transformation. It is worth noting that the proposed transformation in Eq. (3) is the angular analogue of the sector compression along the Cartesian coordinate in [43].

As pointed out previously, the radial anisotropy can be obtained from the coordinate transformation described by the cut and glue process on a homogeneous medium. The Volterra construction indicates the nontrivial topological nature of the radial anisotropy. From the symmetry analysis, the origin is a singular point that lacks a well-defined coordinate transformation for the angular coordinate, which is also a major difference compared to the sector compression in Cartesian coordinates. Let us elucidate this point by examining the total change of the angle θ associated with a closed loop in the original space and its image in the physical space. We consider a closed loop encircling the origin in the xy plane. In the original space, a point moves along the loop for one round and returns to the starting point with 2π angle difference, regardless of how the actual trajectory is distorted. Under the coordinate transformation of Eq. (3), the image of the loop in physical space fails to be closed, and the actual angle difference is $2\pi(1-\alpha)$. This angle is also independent from the actual path, and so it can be viewed as a topological invariant characterizing the topological nature of the geometry. There is a straightforward geometric interpretation for the radial anisotropy: $0 < \alpha < 1$ corresponds to the removal of a wedge with the deficit angle $\Delta\theta = 2\pi\alpha$ from the originally flat space, while $\alpha > 1$ corresponds to the insertion of a wedge into the original space. As is shown in Ref. [41], disclination geometry with $\alpha \neq 1$ describes a curvature singular space where the Riemann curvature tensor is zero everywhere except at the origin, which is given by

$$R_{12}^{12} = 2\pi\frac{1-\alpha}{\alpha}\delta^{(2)}(r), \tag{6}$$

where $\delta^{(2)}(r)$ is the 2D Dirac δ function defined in the xy plane. An immediate consequence of Eq. (6) is that the singular curvature can be either positive or negative depending on the value of α: The curvature is positive if α is a positive real number $0 < \alpha < 1$, while it is negative for the case $\alpha > 1$, and the curvature becomes zero for $\alpha = 1$. In fact, the above observation allows us to define a topological invariant by $1-\alpha$, where the sign indicates a positive or negative topological charge. However, this definition is invalid for imaginary α. In Sec. IV, we will define a general topological invariant based on the semiclassical effective potential acting on the light ray.

In the above geometric analysis, we have theoretically demonstrated the correspondence between radial anisotropy with purely real or purely imaginary α and (pseudo)-Riemannian geometry in relativity physics. In general, any optical material should include loss or gain to fulfill the causality principle. Therefore, α defined by Eq. (1) can be complex valued if loss or gain is taken into consideration. However, the space-time geometry must be real. In the language of transformation optics, this means we always work with real coordinates. Since we are interested in the geometrical aspect of radial anisotropy, we consider only the real part of the permittivity in this work. If the coordinate transformation is generalized to complex coordinates [31,44,45], the transformed material parameters become complex functions of the space coordinates. However, this approach does not describe the effective geometry of the radial anisotropy, since the absorption of radially anisotropic material has nothing to do with the coordinate transformation. Also, whether there is an optical interpretation of complex space-time, which was first proposed by Einstein in 1945 to include an antisymmetric imaginary tensor into the metric $G_{\mu\nu} = g_{\mu\nu} + ib_{\mu\nu}$ for the classical unified field theory [46], is still an open problem.

The singular nature of the curvature indicates that the space of radial anisotropy is locally flat except at the origin. This can be verified from the interpretation of the coordinate transformation based on the Volterra process. Applying the cut and glue process to a paper leads to a 2D cone embedded in three-dimensional flat space with the apex as a singularity. By dropping the last term in the metric in Eq. (2), we can recover the line element of the cone $ds^2 = \sin^{-2}\phi dr^2 + r^2 d\theta^2$. Here, ϕ denotes the half angle of the cone, which links the z coordinate with the radial coordinate r in the spherical polar coordinates (r,θ,z) according to $r = z\tan\phi$. This construction can be confirmed by observing that the deficit angle associated with a cone is given by $2\pi(1-\sin\phi)$, and so we can identify that $\alpha = \sin\phi$. The equivalence of the metric tensors means the physics in a cylindrically radial anisotropic material is topologically identical to the behavior on the conical surface.

The radial anisotropy has two types of metamaterial realizations based on concentric multilayers or radial slices, respectively. The corresponding permittivity for a concentric multilayered metamaterial is given by

$$\varepsilon_\theta = \eta\varepsilon_1 + (1-\eta)\varepsilon_2, \quad \varepsilon_r = \frac{\varepsilon_1\varepsilon_2}{\eta\varepsilon_2 + (1-\eta)\varepsilon_1}, \tag{7}$$

where we define the filling factor of material 1 from $\eta = d_1/(d_1+d_2)$, where d_1 and d_2 are the thicknesses of the materials with dielectric constants ε_1 and ε_2, respectively. Combining Eq. (7) with Eq. (1), we obtain the following expression

$$\alpha^{-2} = 1 + \eta(1-\eta)\left(\sqrt{\frac{\varepsilon_1}{\varepsilon_2}} - \sqrt{\frac{\varepsilon_2}{\varepsilon_1}}\right)^2. \tag{8}$$

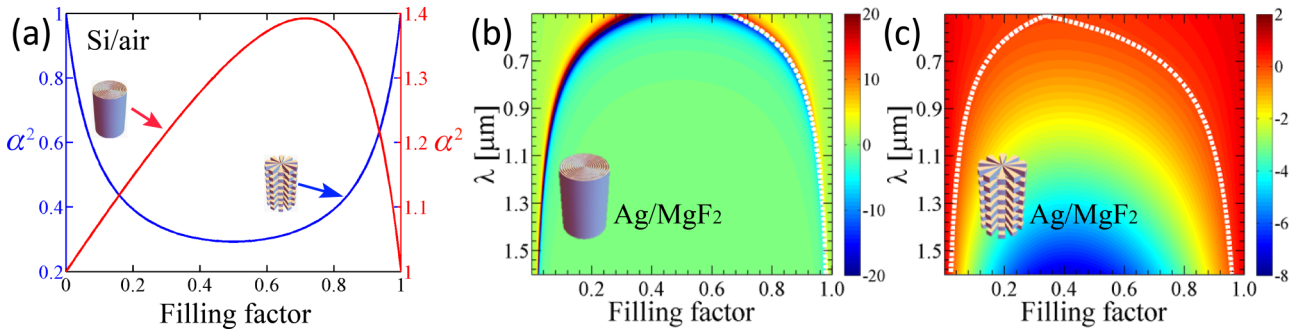

FIG. 2. (a) α^2 versus filling factor for two metamaterials consisting of Si/air concentric multilayers (blue) and radially symmetric slices (red), respectively. Here, we neglect the dispersion of Si, and the permittivity of Si is set to be 11.56 (at 1550 nm). (b, c) Frequency dependence of α^2 on the filling factor for Ag/MgF_2 concentric multilayers (b) and radial slices (c). In (b), the value of α^2 is restricted from -20 to 20.

Since the second term in the right-hand side is nonnegative for a nonabsorbing dielectric medium, the conical parameter α satisfies

$$0 \leqslant \alpha \leqslant 1 \tag{9}$$

for any positive $\varepsilon_1, \varepsilon_2$, and ratio d_1/d_2. Here, the equality $\alpha = 1$ holds for the homogeneous limit $\varepsilon_1 = \varepsilon_2$ or $\eta = 1$. This result can be verified with a specific example of the Si/air system. As shown in Fig. 2(a), $\alpha_{\mathrm{Si/air}}$ is less than 1 and larger than 0.54 for any filling factor. For simplicity, we have neglected the dispersion of Si and chosen the permittivity of Si to be 11.56, i.e., at 1550 nm. For the multilayered metamaterial structure, the minimum value of α can be further decreased if we replace Si with a larger index material.

For the radially sliced medium, the principal values of permittivity are given by

$$\varepsilon_\theta = \frac{(1+\eta)\varepsilon_1\varepsilon_2 + (1-\eta)\varepsilon_2^2}{(1+\eta)\varepsilon_2 + (1-\eta)\varepsilon_1}, \quad \varepsilon_r = \eta\varepsilon_1 + (1-\eta)\varepsilon_2, \tag{10}$$

with ε_1 and ε_2 denoting the permittivity of the wire and the background medium, respectively. In this case, we have $\varepsilon_r \geqslant \varepsilon_\theta$ for any ordinary dielectric with positive permittivity, and it corresponds to the insertion of a sector with

$$\alpha > 1. \tag{11}$$

This can also be verified from the red curve in Fig. 2(a), where a maximal α value of 1.4 is found when the filling factor of Si approaches 0.7. From the above analysis, we find that the two kinds of metamaterial realizations of radial anisotropy correspond to the disclinations by removing or inserting a wedge of constant deficit angle from or into a flat space, respectively.

It has been shown that metamaterials based on ordinary dielectrics with positive indices can realize real disclination parameters depending on the specific geometry. We now turn to the geometry of radial anisotropy with an imaginary α by introducing strong dispersive materials. It is known that α becomes imaginary in some special regions of η and λ when plasmonic metals are included in the metamaterials, indicating a hyperbolic dispersion. For this case, there is no intuitive geometric picture, such as ordinary disclination described above, because the spatial metric is no longer definitely positive when α^2 is negative. Actually, the coordinate with a negative metric component behaves as a timelike coordinate that turns the effective geometry of the radially anisotropic medium from Riemannian space to a pseudo-Riemannian space. This metric signature transition has been reported in the study of hyper metamaterials [47]. Based on the Minkowski-type metric of the hyperbolic metamaterials, analogue relativistic physics can be realized in an optical laboratory [47,48]. Here, we are interested in the dependence of α^2 on the geometric and electromagnetic parameters of the metamaterials in the optical frequencies. Figures 2(b) and 2(c) present the frequency dependence of α^2 on the filling factor for the concentric multilayered structure and the radial wire structures, respectively. In the calculations, we have chosen the constituent materials as Ag and MgF_2, respectively. For bulk Ag, the permittivity is taken from the experimental data [49]. The permittivity of MgF_2, is taken as 1.9. For both geometries, there exist clear regions separating positive and negative α^2. In the multilayered structure [see Fig. 2(b)], the deeply blue region denotes the transition from $-\infty$ to $+\infty$ for α^2 for a filling factor smaller than 0.5 because of $\varepsilon_\theta \to 0$. The dashed white line for filling factor larger than 0.5 denotes $\alpha^2 = 0$ due to $\varepsilon_r \to 0$, and larger values of $|\alpha^2|$ can only be found in the deep color region. It can be found that α^2 is less than -1 in the larger area below the transition region, while it is larger than 1 in the regions above the transition region. Extreme values are found close to the transition region. For the radial sliced medium shown in Fig. 2(c), the dashed white lines denote $\alpha^2 = 0$, which separates the elliptical anisotropy region in the higher frequencies from the hyperbolic anisotropy region in the lower frequencies. It is very interesting to note that the absolute value of α^2 is less than 1 in most of the region (η,λ), and the maximum value $-\alpha^2 = 7.3$ can be realized in a narrow area in the infrared region. These results indicate that we can, in principle, realize arbitrary α in a multilayered structure by varying the filling factor and operating frequency, despite the inevitable absorption and the precise control over the thickness of each layer.

III. WAVE OPTICS IN RADIALLY ANISOTROPIC SPACE

In this section, we consider the wave optics for harmonic waves in the 2D xy plane of a radially anisotropic medium. For TM polarized incidence, the governing equation in curved

space is given by [50]

$$\left(\frac{1}{\sqrt{g}}\partial_\alpha(\sqrt{g}g^{\alpha\beta}\partial_\beta)+k_0^2\right)H_z=0, \tag{12}$$

where $g=\det(g_{\alpha\beta})$, $\nabla^2\equiv\frac{1}{\sqrt{g}}\partial_\alpha(\sqrt{g}g^{\alpha\beta}\partial_\beta)$ is the Laplacian operator in Riemannian space, and $k_0=\omega/c$ is the wave vector in a vacuum. For the radially anisotropic medium with 2D metric $g_{\alpha\beta}=\mathrm{diag}(1,\alpha^2r^2)$, the contravariant metric takes the form $g^{\alpha\beta}=\mathrm{diag}(1,\alpha^{-2}r^{-2})$. With this, the wave equation takes the following form

$$\left(\frac{1}{r}\frac{\partial}{\partial r}r\frac{\partial}{\partial r}+\frac{\partial}{\partial\theta}\frac{1}{\alpha^2r^2}\frac{\partial}{\partial\theta}+k_0^2\right)H_z=0. \tag{13}$$

Assuming the geometric parameter α is independent from r and considering the solution of the form $H_z\propto\psi(r)\exp(im\theta)$, we arrive at the following Bessel equation

$$\left(r^2\frac{\partial^2}{\partial r^2}+r\frac{\partial}{\partial r}+\left(k_0^2r^2-\frac{m^2}{\alpha^2}\right)\right)\psi(r)=0. \tag{14}$$

Here, $\psi(r)$ is the radial part of the magnetic field H_z, m is the angular momentum mode number of the cylindrical waves. Equation (14) is just the well-known wave equation for radial anisotropy despite an overall factor ε_θ inside the brackets. The solutions of the above equation are Bessel functions:

$$\begin{aligned}\psi(r)&=c_1J_{m/\alpha}(k_0r)+c_2Y_{m/\alpha}(k_0r), \quad \text{if} \quad \alpha^2>0,\\ \psi(r)&=c_3I_{m/\alpha}(k_0r)+c_4K_{m/\alpha}(k_0r), \quad \text{if} \quad \alpha^2<0,\end{aligned} \tag{15}$$

where $(J_{m/\alpha}(k_0r),Y_{m/\alpha}(k_0r))$ and $(I_{m/\alpha}(k_0r),K_{m/\alpha}(k_0r))$ are the ordinary and modified Bessel functions of the first and second kind, respectively. These solutions turn into the ordinary Bessel function solutions in a flat space where $\alpha=1$. The geometric picture of radial anisotropy not only gives an alternative approach in deriving the wave Eq. (14), but it also provides a geometric interpretation of the resolution limit of the cylindrical (super)lens made from a radially anisotropic medium. To be specific, we follow the analysis of the optical hyperlens presented in [5]. A conventional lens is subject to Abbe's diffraction limit due to the uncertainty principle, and it cannot reconstruct the image of an object with feature size below $\lambda/2$ [51]. To overcome the diffraction limit, it needs to convey information carried by a large wave vector component to the far field. As shown in [5], the solutions $H_z\propto\psi(r)\exp(im\theta)$ with various m values can be considered as distinct channels of various angular momentums. It is known that the higher order ordinary Bessel function decays exponentially at the origin, leading to vanishing coupling between the higher angular momentum channels and the object inside the radius of the caustic

$$R_c\propto m\lambda.$$

From the geometric viewpoint, the nontrivial radial anisotropy with $\alpha\neq1$ leads to a factor on the order of the Bessel function from m to m/α. This nontrivial factor can be directly understood from the scale transformation on the angular coordinate of the coordinate transformation. Specifically, the caustic radius R_c decreases if $\alpha>1$ for a given angular momentum mode m, while R_c increases if $0<\alpha<1$, which can be found for various $\alpha=0.7$, 1, and 1.3 as shown in Fig. 3. As a result, a larger α leads to a stronger coupling between the higher order angular momentum mode and the object. Consequently, a concentric layered structure based on ordinary dielectrics decreases the resolution limit because its conical parameter less than 1. On the contrary, the resolution limit will increase for sliced structures. For hyperbolically radial anisotropy, the parameter becomes imaginary $\alpha=i|\alpha|$. As a result, the solution changes from the ordinary Bessel function, which diverges at the origin, and leads to a strong coupling between the information channels of higher angular momentum with the object, thereby giving rise to the far field superlensing effect.

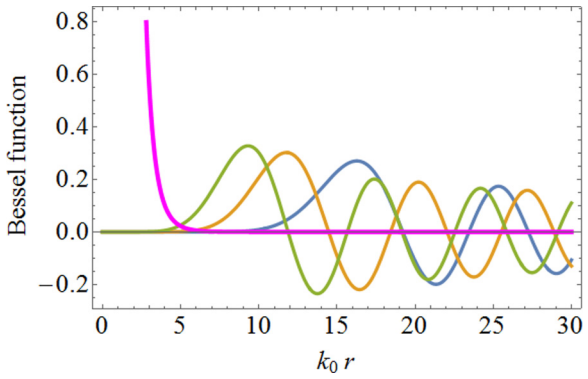

FIG. 3. Ordinary Bessel functions $J_{m/\alpha}(k_0r)$ of order m/α for $m=10$ and $\alpha=0.7$ (blue), $\alpha=1$ (orange), and $\alpha=1.3$ (green). The blue line indicates the modified Bessel function of the second kind $K_{m/\alpha}(k_0r)$ of order m/α with $m=10$ and $\alpha=2.2$, which corresponds to solutions in hyperbolically radial anisotropy.

It is interesting to note that the azimuth transformation supplemented with suitable radial coordinate transformation can be used for designing a subwavelength cavity which traps electromagnetic fields inside a subwavelength-bounded region [52,53]. As pointed out above, the azimuth transformation relates the radial part of the solutions in vacuum and in transformed space with a factor α^{-1} for the order of the Bessel functions. Mathematically, the factor can be moved to the angular part, i.e.,$\exp(im\theta)\rightarrow\exp(im\theta/\alpha)$ while keeping the radial part argument invariant. In this regard, the azimuth mode in the transformation region is different from the mode in the neighboring vacuum region. Consequently, a single azimuth mode in the subwavelength cavity in general can be used to excite multiple azimuth modes in the vacuum region and vice versa [53].

IV. RAY DYNAMICS IN RADIALLY ANISOTROPIC SPACE

In the present section, we analyze the ray dynamics of a narrow light beam in a medium with cylindrical anisotropy in the framework of transformation optics. For simplicity, we only consider the equation of motion in a 2D xy plane, since the supposed translational invariance in the z axis introduces no new effects for light propagation. To fulfill the geometric optics approximation, it is assumed that the effect of curvature is small compared to the incident wavelength, i.e., the characterized dimension of the metamaterial structure is much smaller than λ. It should be pointed out that this condition does not hold for large radius. We first derive the geodesic

equation in curved space from the straight-line trajectory in a homogeneous medium with the help of coordinate transformation. A light ray in a homogeneous medium or a flat space follows the straight-line equation, which is defined by the parameter equation

$$\ddot{x}^a = 0, \tag{16}$$

where "." stands for $\partial/\partial t$. Under a coordinate transformation: $x^a \to x^\alpha(x^a)$ $(a,\alpha = 1,2,3)$, Eq. (16) can be easily transformed to physical space by employing the chain rule:

$$\ddot{x}^\gamma + \Gamma^\gamma_{\alpha\beta}\dot{x}^\alpha\dot{x}^\beta = 0, \tag{17}$$

where $\Gamma^\gamma_{\alpha\beta} = \frac{\partial x^\gamma}{\partial x^a}\frac{\partial^2 x^a}{\partial x^\alpha \partial x^\beta}$. Rewrite $\Gamma^\gamma_{\alpha\beta} = \boldsymbol{e}^\gamma \cdot \partial_\beta \boldsymbol{e}_\alpha$ with $\boldsymbol{e}^\gamma = \Lambda^\gamma_a \boldsymbol{e}^a$, and we can find that $\Gamma^\gamma_{\alpha\beta}$ turns to be the usual Christoffel symbol of the second kind in Riemannian physical space: $\Gamma^\gamma_{\alpha\beta} = 1/2 g^{\gamma\delta}(\partial_\alpha g_{\beta\delta} + \partial_\beta g_{\alpha\delta} - \partial_\delta g_{\alpha\beta})$ [50], if the physical space is torsionless or the coordinate transformation is integrable, i.e., $\partial_\alpha \Lambda^a_\beta - \partial_\beta \Lambda^a_\alpha = 0$. Here, $\boldsymbol{e}^a = (\boldsymbol{i},\boldsymbol{j},\boldsymbol{k})$ denote the basic vectors in the original Cartesian system satisfying $\boldsymbol{e}^a \cdot \boldsymbol{e}^b = \delta^{ab}$. It should be pointed out that although we are working with Cartesian coordinates in arriving at Eq. (17), the geodesic equation holds for any holonomic curvilinear system. This means the equation of motion is the geodesic equation in curved space as well as in flat space with curvilinear coordinates [50]. For the disclination metric, the nonzero Christoffel symbols are $\Gamma^r_{\theta\theta} = -\alpha^2 r$ and $\Gamma^\theta_{r\theta} = \Gamma^\theta_{\theta r} = r^{-1}$. From the nonzero components of $\Gamma^\gamma_{\alpha\beta}$, we obtain the coupled equations of motion in polar coordinate:

$$\ddot{r} - \alpha^2 r\dot{\theta}^2 = 0, \quad \ddot{\theta} + 2\dot{r}\dot{\theta} = 0. \tag{18}$$

These equations indicate that the motion of a light beam due to radial anisotropy is similar to the orbital motion of a classical charged particle in a central Coulomb potential. In addition, the first integrals from angular momentum and total energy conservation for these two equations are

$$\alpha^2 r^2\dot{\theta} = L, \quad \frac{\dot{r}^2}{2} + \frac{L^2}{2\alpha^2 r^2} = E, \tag{19}$$

where the integral constants L and E are the angular momentum and energy of the system [54], respectively.

Before analyzing the ray dynamics in detail, we pay attention to the first integral of energy conservation. From the radial kinetic energy in Eq. (19), the photon can be regarded as a charged particle, while the effective potential is an inverse square function of the radius $V'(r) = L^2/2\alpha^2 r^2$. To gain deep physical insights on the features of the light ray, we separate the rotational energy from the potential according to

$$V'(r) = \frac{L^2}{2r^2} + V(r), \tag{20}$$

where $L^2/2r^2$ is the rotational energy of the point particle appearing in polar coordinates [48], and the real potential $V(r)$ is thus given by

$$V(r) = \frac{1-\alpha^2}{\alpha^2}\frac{L^2}{2r^2}. \tag{21}$$

Obviously, the potential can be attractive or repulsive, depending on the value of α^2. If $\alpha^2 < 0$, the potential is negative, and so it represents an attractive potential for the test photon. At the same time, the metric gives rise to a pseudo-Riemannian geometry. We can identify that the effective geometry of the anisotropic medium is similar to a pseudocone: If $0 < \alpha^2 < 1$, the potential is still attractive; however, the metric tensor describes the geometry of a hyperbolic cone that corresponds to a negative curvature singularity. If $\alpha^2 > 1$, the potential is repulsive, which corresponds to an ordinary conic geometry. It can also be found that the beam follows a spiral-like trajectory despite the strongly anisotropic scattering due to the failure of the effective medium model at larger radius for sectored geometry. Consequently, we can define the following topological charge

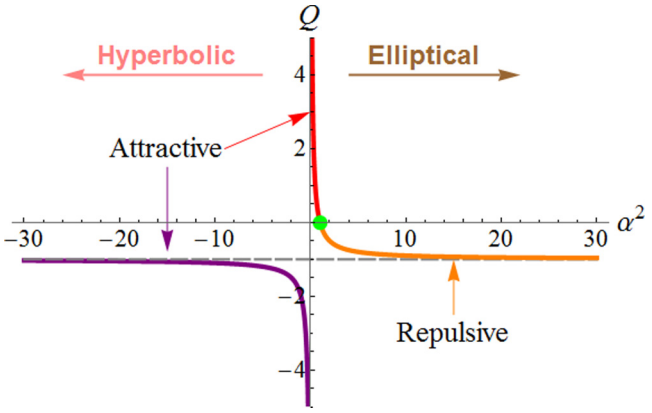

FIG. 4. Dependence of the topological charge on the parameter α^2, where the green dot indicates zero topological charge Q when $\alpha = 1$. Different colors in the curves indicate attractive (red, purple) or repulsive (orange) potentials.

$$Q = \frac{1-\alpha^2}{\alpha^2}. \tag{22}$$

The above definition is a direct generalization of the topological charge defined in Ref. [41]. From the potential $V(r)$, we find that a medium with topological charge Q acts on the light similar to the motion of a charged particle in a Coulomb potential. Obviously, the definition in Eq. (22) can be applied for either real or imaginary α. The dependence of Q on the geometric parameter α^2 is depicted in Fig. 4. It is found that the topological charge is positive only if $0 < \alpha^2 < 1$; it is negative when $\alpha > 1$ or α is imaginary. By analogue with the motion of the point particle in the classical Kepler problem, the semiclassical dynamics of the photon in a positive charge system are totally different than the motion in the potential with negative topological charge.

Because the real potential is a power-law function of radial distance of order -2, $V(r) \propto r^{-2}$, the concentric force $F(r) \propto r^{-3}$, which is different than an inverse square force such as gravity or electrostatic force. Physically, only the power-law attractive force with order $n > -3$ is capable of stable circular orbits [54]. As a result, the radial anisotropy does not support stable closed orbits for light rays. In principle, the motion equation can be solved from the conservation laws. However, the equation of motion for the light ray studied here can be directly obtained from the coordinate transformation from the rays in the original space without solving the differential equations. In polar coordinates, the straight-line equation takes

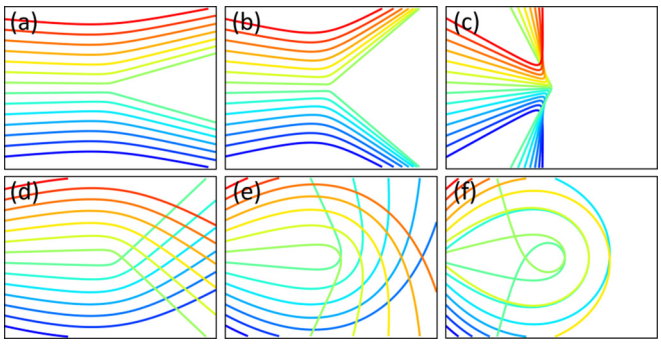

FIG. 5. Ray tracing for photon in a space with different conical parameters: (a–c) $\alpha = 1.1,\ 1.3,$and 3; (d–f) $\alpha = 0.8,\ 0.6,$and 0.4.

the following form

$$r\cos(\theta - \theta_0) = r_0, \tag{23}$$

where $r_0 = L/\sqrt{2E}$. With the coordinate transformation in Eq. (3) with nontrivial α, we can obtain the motion equation by making the substitution $\theta \to \alpha\theta$ as we have done for the wave dynamics. Explicitly, the geodesics in physical space are given by

$$\begin{aligned} \alpha r\cos(\alpha[\theta - \theta_0]) &= r_0, \quad \text{if} \quad \alpha^2 > 0, \\ |\alpha| r\cosh(|\alpha|[\theta - \theta_0]) &= r_0, \quad \text{if} \quad \alpha^2 < 0. \end{aligned} \tag{24}$$

Here, we have made the substitution $\cos\alpha\theta \to \cosh|\alpha|\theta$ for imaginary α and yield the corresponding geodesic equation. Equation (24) with cosh describes the spirallike trajectory for light in a hyperbolically radial anisotropic medium, which has been previously reported [6], while the trajectories in elliptically radial media are open orbitals. Here, we emphasize that the spiral motion has the same geometric origin as the case of ordinary radial anisotropy.

From the above nonradial geodesic equations, we can solve the trajectories of light rays in a radially anisotropic medium. Because the spiral motion has been studied in the context of a perfect lens [8], here we only focus on the case of positive α. According to the analysis in Sec. II, a positive α has an intuitive geometric meaning: $\alpha > 1$ corresponds to inserting a wedge, while $0 < \alpha < 1$ results from removing a wedge from flat space. In this geometric scenario, a straight line, which represents the light ray in the original flat space, is bent away from the singularity when a wedge is inserted, indicating a repulsive potential. In contrast, the straight line is bent inwards to the singularity when a wedge is removed, indicating an attractive potential. This geometric analysis is consistent with the classification of topological charges where Q has opposite signs for $0 < \alpha < 1$ and $\alpha > 1$. To verify the intuitive analysis, we present the trajectories of light rays in media with different positive α. The solutions are numerically solved with the particle tracing module of the commercial finite element method solver Comsol. As predicted, the ray can be repelled or attracted by the origin, following a series of orbits depending on the incident direction and the different arguments in the cos or cosh functions. Figures 5(a)–5(c) show the ray dynamics for a medium with $\alpha = 1.1$, 1.3, and 3, respectively. It is found that the light ray is repelled by the singularity, and the deflection angle increases with α. In addition, an important feature for $\alpha > 1$ is that, by the geometric construction, there exist two asymptotes that are equal to one half of the deficit angle. Parallel light rays coming from the left would never enter the region bounded by the asymptotes. For $0 < \alpha < 1$, the light ray is attracted by the radial anisotropy because of the removal of a wedge from the flat space, which can be seen in Figs. 5(d)–5(f), where α is 0.8, 0.6, and 0.4, respectively. It is interesting to notice that the light ray can make a turn around the defect for small α while the orbit is still open.

To further validate the theoretical analysis, we performed full-wave electromagnetic simulations using the RF module of Comsol. In Figs. 6(a)–6(c), we present the propagation of a TM polarized Gaussian beam in concentric multilayered structures of dielectrics with varied α. In the calculation, the incident

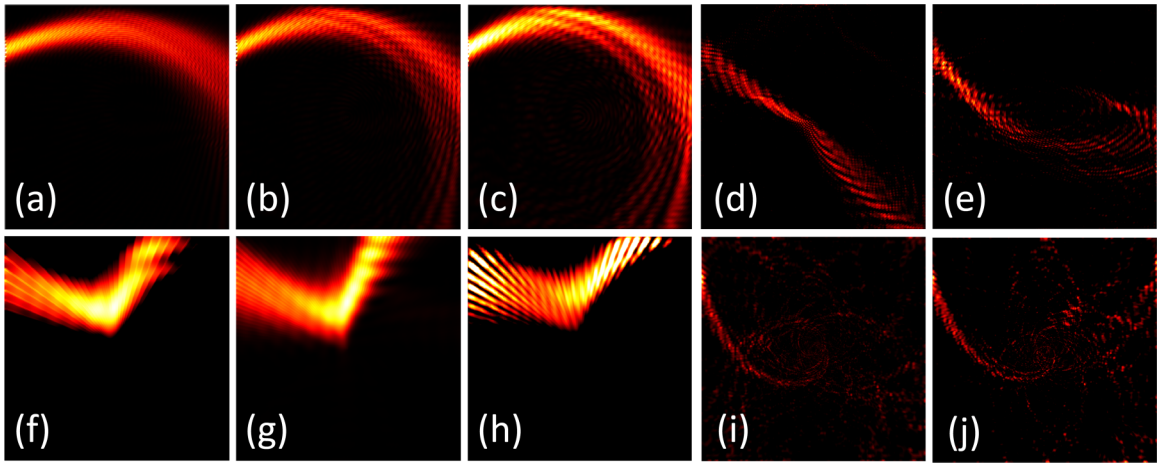

FIG. 6. Full-wave simulated $|H|^2$ distribution of a light beam in concentric multilayered structures (a–e) and symmetric sliced structures (f–j), both with varied α. The structure parameters in (a–c) are d_1:d_2 = 1:5,1:2, and 1:1, and the values of permittivity are $\varepsilon_1 = 1$ and $\varepsilon_2 = 11.56$. The corresponding α is 0.6537, 0.564, and 0.5414, respectively. In (d), $\alpha = 2.4i$, d_1:d_2 = 1:1, $\varepsilon_1 = 0.9$, and $\varepsilon_2 = -0.4$. In (e), $\alpha = 1.333i$, d_1:d_2 = 1:1, $\varepsilon_1 = 1.6$, and $\varepsilon_2 = -0.4$. (f–h) The structure parameters of the symmetric slices are: θ_1:θ_2 = 3:1,1:1, and 1:3, and the values of permittivity are $\varepsilon_1 = 1$ and $\varepsilon_2 = 11.56$. The corresponding α is 1.1789, 1.1538, and 1.0874, respectively. In (i), $\alpha = 1.975i$, θ_1:θ_2 = 1:1, $\varepsilon_1 = 1$, and $\varepsilon_2 = -2.5$. In (j), $\alpha = 4.15i$, θ_1:θ_2 = 1:1, $\varepsilon_1 = 1.4$, and $\varepsilon_2 = -4$.

wavelength is chosen to be 1600 nm, the lattice spacing along the radial direction $d_1 + d_2$ is 160 nm, and the thickness ratios for materials 1 and 2 are d_1:d_2 = 1:5, 1:2, and 1:1, respectively. Here, we only consider a moderate aspect ratio that can be realistically implemented with nanofabrication methods. The two constituent materials are chosen to be air and Si, and the corresponding geometric parameter α is 0.6537, 0.564, and 0.5414, respectively. It is shown that the beam is attracted by the singularity as the motion of a massive point particle in a central gravitational field. The observed attraction is in agreement with Volterra's construction of the cone with $\alpha < 1$ by removing a wedge from a flat space. As the filling factor increases, the curvature radius of the trajectory becomes larger. Here, a smaller α indicates a sharper disclination, hence bending light stronger. For comparison, we present the light propagation in Si/air symmetric sliced metamaterial structures with different angle ratios 1:3, 1:1, and 3:1 in Figs. 6(f)–6(h). The corresponding α is 1.179, 1.154, and 1.1, respectively. It is found that the reflection angle decreases with the filling factor as expected. Contrary to the open orbits in the elliptical region shown in Figs. 6(a)–6(c) and 6(f)–6(h), the trajectories follow Poinsot spirals inside the hyperbolically radial anisotropic media for imaginary α. Figures 6(d) and 6(e) show the propagation of a light beam by radially anisotropic media consisting of alternative concentric multilayers of the same thickness. Here, the permittivity of material 2 is $\varepsilon_2 = -0.4$, while that of material 1 is $\varepsilon_1 = 0.9$ and $\varepsilon_1 = 1.6$, respectively. It is found that the beam is attracted to cross the origin with a spirallike trajectory. Similarly, the scattering of light beams in the hyperbolically sliced metamaterials with the same angle is shown in Figs. 6(i) and 6(j). Here, the permittivity of material 1 is chosen as $\varepsilon_1 = 0.4$, while $\varepsilon_2 = -2.5$ and $\varepsilon_2 = -4$, respectively. It should be pointed out that it is not a good approximation to regard the beam as a light ray of zero size when the beam is close to the origin because of the following reasons: First, the anisotropy varies strongly near the origin, which gives rise to an anisotropic response for the different regions of the beam. Second, the beam can overlap the origin due to the beam's finite width, by which the light can re-emit from the origin as shown in Fig. 6(d).

V. CONCLUSIONS

In summary, we have presented a geometrical interpretation for the optical response of radially anisotropic materials from the viewpoint of transformation optics. It is shown that the radial anisotropy resembles the curved geometry of the line topological defect known as disclination, with the origin behaving as a topological singularity. We have systematically investigated the effective geometry for radially anisotropic metamaterials consisting of concentric multilayers and symmetric slices. Depending on the parameter selection, the radial anisotropy can be equivalent to Riemannian geometry or pseudo-Riemannian geometry. The associated topological charge determines the optical properties from wave optics as well as ray dynamics and provides an alternative explanation for the radially anisotropic lens and beam steering with radial anisotropy. Our theory not only gives a geometric view for radial anisotropy, but also an approach to control electromagnetic waves with topological nontrivial configurations beyond the well-known vortices from computer-generated holograms, and it is excepted that the same scheme can also be applied to the other classical and quantum systems.

ACKNOWLEDGMENT

This work was financially supported by the Hong Kong Polytechnic University (Grant No. 1-ZE23) and the National Natural Science Foundation of China (Grant No. 11474240).

[1] J. Roth and M. J. Dignam, Scattering and extinction sections for a spherical particle coated with an oriented molecule layer, J. Opt. Soc. Am. **63**, 308 (1973).

[2] M. Kociak, O. Stephan, L. Henrard, V. Charbois, A. Rothschild, R. Tenne, and C. Colliex, Experimental Evidence of Surface Plasmon Coupling in Anisotropic Hollow Nanoparticles, Phys. Rev. Lett. **87**, 075501 (2001).

[3] S. Zummer, Light scattering from nematic droplets: Anomalous diffraction approach, Phys. Rev. A **37**, 4006 (1988).

[4] H. Karacali, S. M. Risser, and K. F. Ferris, Scattering of light from small nematic spheres with radial anisotropy, Phys. Rev. E **56**, 4286 (1997).

[5] A. Poddubny, I. Iorsh, P. Belov, and Y. Kivshar, Hyperbolic metamaterials, Nat. Photon. **7**, 948 (2013).

[6] P. Shekhar, J. Atkinson, and Z. Jacob, Hyperbolic metamaterials: Fundamentals and applications, Nano Converg. **1**, 14 (2014).

[7] Z. Jacob, L. V. Alekseyev, and E. Narimanov, Optical hyperlens: Far field imaging beyond the diffraction limit, Opt. Express **14**, 8247 (2006).

[8] Z. Jacob, L. V. Alekseyev, and E. Narimanov, Semiclassical theory of the hyperlens, J. Opt. Soc. A **24**, A52 (2007).

[9] J. Rho, Z. Ye, Y. Xiong, X. B. Yin, Z. W. Liu, H. Choi, G. Bartal, and X. Zhang, Spherical hyperlens for two dimensional sub-diffraction imaging at visible frequencies, Nat. Commun. **1**, 143 (2010).

[10] I. I. Smolyaninov, Y. J. Hung, and C. C. Davis, Imaging and focusing properties of plasmonic metamaterial devices, Phys. Rev. B **76**, 205424 (2007).

[11] S. Tretyakov, P. Alitalo, O. Luukkonen, and C. Simovski, Broadband Electromagnetic Cloaking of Long Cylindrical Objects, Phys. Rev. Lett. **103**, 103905 (2009).

[12] C. W. Qiu, L. Hu, X. F. Xu, and Y. J. Feng, Spherical cloaking with homogeneous isotropic multilayered structures, Phys. Rev. E **79**, 047602 (2009).

[13] H. Kettunen, H. Wallen, and A. Sihvola, Cloaking and magnifying using radial anisotropy, J. Appl. Phys. **114**, 044110 (2013).

[14] C. W. Qiu, L. Gao, J. D. Joannopoulos, and M. Soljacic, Light scattering from anisotropic particles: Propagation, localization and nonlinearity, Laser Photon. Rev. **4**, 268 (2010).

[15] J. W. Jin, D. L. Gao, and L. Gao, Plasmonic resonant light scattering by a cylinder with radial anisotropy, Prog. Electro. Res. **106**, 335 (2010).

[16] H. L. Chen and L. Gao, Anomalous electromagnetic scattering from radially anisotropic nanowire, Phys. Rev. A **86**, 033825 (2016).
[17] H. Wallen, H. Kettunen, and A. Sihvola, Anomalous absorption, plasmonic resonances and invisibility of radially anisotropic spheres, Radio Sci. **50**, 18 (2015).
[18] J. Pendry, D. Schurig, and D. R. Smith, Controlling electromagnetic fields, Science **312**, 1780 (2006).
[19] U. Leonhardt, Optical conformal mapping, Science **312**, 1777 (2006).
[20] H. Y. Chen, C. T. Chan, and P. Sheng, Transformation optics and metamaterials, Nat. Mat. **9**, 387 (2010).
[21] J. B. Pendry, A. Aubry, D. R. Smith, and S. A. Maier, Transformation optics and subwavelength control of light, Science **337**, 549 (2012).
[22] D. Shurig, J. J. Mock, B. J. Justice, S. A. Cummer, J. B. Pendry, A. F. Starr, and D. R. Smith, Metamaterial electromagnetic cloak at microwave frequencies, Science **314**, 977 (2006).
[23] W. S. Cai, U. K. Chettiar, A. V. Kildishev, and V. M. Shalaev, Optical cloaking with metamaterials, Nat. Photon. **1**, 224 (2007).
[24] J. Valentine, J. Li, T. Zentgraf, G. Bartal, and X. Zhang, An optical cloak made of dielectrics, Nat. Mat. **8**, 568 (2009).
[25] R. Liu, C. Ji, J. Mock, J. Chin, T. J. Cui, and D. R. Smith, Broadband ground-plane cloak, Science **323**, 366 (2009).
[26] B. Zhang, Y. Luo, X. Liu, and G. Barbastathis, Macroscopic Invisibility Cloak for Visible Light, Phy. Rev. Lett. **106**, 033901 (2011).
[27] Y. Lai, J. Ng, H. Y. Chen, D. Z. Han, J. J. Xiao, Z. Q. Zhang, and C. T. Chan, Illusion Optics: The Optical Transformation of an Object into Another Object, Phys. Rev. Lett. **102**, 253902 (2009).
[28] N. B. Kundtz and D. R. Smith, Extreme-angle broadband metamaterial lens, Nat. Mater. **9**, 129 (2010).
[29] M. W. McCall, A. Favaro, P. Kinsler, and A. Boardman, A spacetime cloak, or a history editor, J. Opt. **13**, 024003 (2011).
[30] S. A. Tretyakov, I. S. Nefedov, and P. Alitalo, Generalized field-transforming metamaterials, New J. Phys. **10**, 115028 (2008).
[31] G. Castaldi, S. Savoia, V. Galdi, A. Alu, and N. Engheta, PT Metamaterials via Complex-Coordinate Transformation Optics, Phys. Rev. Lett. **110**, 173901 (2013).
[32] L. Bergamin, P. Alitalo, and S. A. Tretyakov, Nonlinear transformation optics and engineering of the Kerr effect, Phys. Rev. B **84**, 205103 (2011).
[33] O. Paul and M. Rahm, Covariant description of transformation optics in nonlinear media, Opt. Express **20**, 8982 (2012).
[34] C. Garcia-Meca and C. Barcelo, Nontensorial Transformation Optics, Phys. Rev. Appl. **5**, 064008 (2016).
[35] G. Castaldi, V. Galdi, A. Alu, and N. Engheta, Nonlocal Transformation Optics, Phys. Rev. Lett. **108**, 063902 (2012).
[36] J. J. Zhang, M. Wubs, P. Ginzburg, G. Wurtz, and A. V. Zayats, Transformation quantum optics: Designing spontaneous emission using coordinate transformations, J. Opt. **18**, 044029 (2016).
[37] S. A. R. Horsley, I. R. Hooper, R. C. Mitchell-Thomas, and O. Quevedo-Teruel, Removing singular refractive indices with sculpted surface, Sci. Reports **4**, 4876 (2014).
[38] R. Balian, M. Kleman, and J. P. Poirier, *Physics of Defects* (North-Holland, Amsterdam, 1981).
[39] M. O. Katanaev and I. V. Volvich, Theory of defects in solids and three dimensional gravity, Ann. Phys. (N. Y.) **216**, 1 (1992).
[40] R. A. Puntugam and H. H. Soleng, Volterra distortions, spinning strings and cosmic strings, Class. Quantum Grav. **14**, 1129 (1997).
[41] Y. L. Zhang, X. Z. Dong, M. L. Zheng, Z. S. Zhao, and X. M. Duan, Steering electromagnetic beams with conical curvature singularities, Opt. Lett. **40**, 4783 (2015).
[42] W. S. Cai, U. K. Chettiar, A. V. Kildishev, and V. M. Shalaev, Designs for optical cloaking with high-order transformation, Opt. Express **16**, 5444 (2008).
[43] J. Pendry, Taking the wraps off cloaking, Physics **2**, 95 (2009).
[44] B. I. Papa and S. A. Cummer, Complex coordinates in transformation optics, Phys. Rev. A **84**, 063837 (2011).
[45] S. Savoia, G. Castaldi, and V. Galdi, Complex-coordinate non-Hermitian transformation optics, J. Opt. **18**, 044027 (2016).
[46] A. Einstein, A generalization of the relativistic theory of gravitation, Ann. Math. **46**, 578 (1945).
[47] I. I. Smolyaninov and E. E. Narimanov, Metric Signature Transitions in Optical Metamaterials, Phys. Rev. Lett. **105**, 067402 (2010).
[48] I. I. Smolyaninov, E. Hwang, and E. Narimanov, Hyperbolic metamaterial interfaces: Hawking radiation from Rindler horizons and spacetime signature transitions, Phys. Rev. B **85**, 235122 (2012).
[49] P. B. Johnson and R. W. Christy, Optical constants of the noble metals, Phys. Rev. B **6**, 4370 (1972).
[50] M. P. Hobson, G. P. Efstathiou, and A. N. Lasenby, *General Relativity: An Introduction for Physicists* (Cambridge University Press, Cambridge, UK, 2006).
[51] L. Novotny and B. Hecht, *Principles of Nano-Optics*, 2nd ed. (Cambridge University Press, Cambridge, UK, 2012).
[52] V. Ginis, P. Tassin, C. M. Soukoulis, and I. Veretennicoff, Confining light in deep subwavelength electromagnetic cavities, Phys. Rev. B **82**, 113102 (2010).
[53] V. Ginis, P. Tassin, J. Danckaert, C. M. Soukoulis, and I. Veretennicoff, Creating electromagnetic cavities using transformation optics, New J. Phys. **14**, 033007 (2012).
[54] H. Goldstein, C. Poole, and J. Safko, *Classical Mechanics*, 3rd ed. (Addison Wesley, Reading, MA, 2001).